

Comparison of Simulated and Measured Drift Scans for Broadband Dipole Antennas at Long Wavelength Array (LWA) Frequencies

Aaron Kerkhoff (ARL:UT)

07/23/2007

The results of a recent effort to compare the sky noise power received by broadband dipole antennas at LWA frequencies as predicted by simulation and given by measurement are summarized. The simulation method, which combines results from a full-wave simulation of a given antenna design with a properly frequency-scaled all-sky map of radio continuum to generate predicted drift scans is first described. The measurement approach, which consists of conducting calibrated total power measurements of the antenna design over an extended period of time, is described. The measured and simulated drift scan results are then compared to determine the level of absolute agreement achieved between the two. Finally, conclusions are given.

Drift Scan Simulation Approach

The predicted variation in received sky noise with time is calculated in the usual manner by convolving simulated radiation patterns for an antenna with an all-sky map. In particular, the equivalent noise temperature due to sky noise for a lossless antenna at a given time, t (in LST), is given by the following expression [1]

$$T_{ANT,lossless}(t) = \frac{1}{\sum_i \sum_j U(\theta, \phi) \cos b} \sum_i \sum_j M(i, j) U(\theta, \phi) \cos b$$

where M denotes the all-sky map, i and j are the map indices, respectively, of galactic latitude and longitude, U is the normalized power pattern of the antenna, θ and ϕ are the elevation and azimuth, respectively, relative to the frame of the antenna and corresponding to the direction given by i and j at time t , and b is the galactic latitude. To determine the temperature received by a real antenna, the following expression is used

$$T_{ANT} = \frac{T_{ANT,lossless} (1 - |\rho|^2)}{L_{gnd}}$$

where $(1 - |\rho|^2)$ is the loss due to mismatch between the antenna and the impedance presented by the pre-amp, and L_{gnd} is loss due to the ground. Ground loss is calculated as the ratio of the total power radiated by the antenna to the total power input to the antenna, P_{rad}/P_{in} , where

$$P_{rad} = \frac{1}{2\eta_0} \int_0^{2\pi} \int_0^\pi (|E^\theta(\theta, \phi)|^2 + |E^\phi(\theta, \phi)|^2) \sin \theta d\theta d\phi;$$

$$P_{in} = \frac{|V_{in}|^2}{2} \operatorname{Re} \left\{ \frac{1}{Z_{in}} \right\}.$$

In the above expressions, η_0 is the free space wave impedance, E^θ and E^ϕ , are the components of the far-field electric field radiated by the antenna, and V_{in} and Z_{in} are the antenna excitation voltage and input impedance, respectively.

The Haslam 408 MHz all-sky map [2] is used in this study. A FITS formatted file containing this map in galactic coordinates was obtained from [3]. The fv FITS reader [4] was used to open this file and generate an ASCII text version for use in simulation. Two approaches are considered for scaling the 408 MHz map down to the LWA frequency range of 20 MHz to 80 MHz, though both methods involve scaling all of the pixels in the map by an equal amount. In the first approach, which will hereafter be called the “original map scaling scheme”, the map is scaled from the map frequency, f_{MAP} , to the observing frequency, f_{OBS} , by a single scaling factor in the following manner

$$M_{scaled,1}(f_{OBS}) = M \left(\frac{f_{OBS}}{f_{MAP}} \right)^{-\beta_0}$$

where β_0 is the chosen spectral index. This approach was used in [5], and good agreement was achieved between simulated and measured drift scans when scaling the 408 MHz map down to 38 MHz using a spectral index of $\beta_0 = 2.55$; this value of β_0 was used in the present study.

In another approach, which will hereafter be called the “alternative map scaling scheme”, contributions to the measured sky noise due to the galactic component, extra-galactic component, and the cosmic microwave background are handled separately in the frequency scaling. This approach is summarized by the following procedure:

- Subtract some assumed values due to an isotropic extra-galactic component at the map frequency, and an isotropic component due to the cosmic microwave background from the original map. The resulting map is mostly due to the galactic component.
- Scale this new map to f_{OBS} by an appropriate spectral index for the galactic component.
- Scale the extra-galactic component to f_{OBS} using an appropriate spectral index (possibly different than that for galactic components).
- Generate the new map by adding the scaled extra-galactic component and cosmic microwave background back to the scaled galactic component map.

In [6], the results from a number of surveys of the radio continuum performed at various frequencies are used to determine the variation in spectral indices as a function of position in the sky and frequency in the northern celestial hemisphere. Using surveys performed at 38 MHz and 408 MHz, a mean spectral index (over all positions in the sky) of roughly 2.6 between those two frequencies for the galactic component was determined. Surveys performed at 17.5 MHz and 81.5 MHz indicate that a mean spectral index for the galactic component of 2.4 is more appropriate between those frequencies. A similar mean value was determined between 38 MHz and 178 MHz surveys suggesting that this value may be valid over the entire range of 17.5 MHz to 178 MHz. On the other hand, a spectral index of roughly 2.75 was determined for the isotropic extra-galactic component; this value is assumed to be relatively constant between 408 MHz and low-end of the LWA band. Using this data, the alternative map scaling can be calculated using

$$M_{scaled,2}(f_{OBS}) = [M - T_0 - T_1(f_{MAP})] \left(\frac{f_{INT}}{f_{MAP}} \right)^{-\beta_1} \left(\frac{f_{OBS}}{f_{INT}} \right)^{-\beta_2} + T_1(f_{MAP}) \left(\frac{f_{OBS}}{f_{MAP}} \right)^{-\beta_3} + T_0 .$$

The definitions and assumed values for parameters in the previous equation are given in Table 1.

Table 1. Parameters used in alternative sky map scaling scheme.

parameter	value	Definition
T_0	2.7 K	Equivalent noise temperature of cosmic microwave background component
$T_1(f_{\text{MAP}})$	3.2 K at 408 MHz	Equivalent noise temperature of isotropic extra-galactic component at frequency of sky map
f_{INT}	38 MHz	Intermediate frequency. Initial frequency scaling of galactic component applied between f_{MAP} and f_{INT} . Secondary scaling applied between f_{INT} and f_{OBS}
β_1	2.6	Spectral index used for initial scaling of galactic component
β_2	2.4	Spectral index used for secondary scaling of galactic component
β_3	2.75	Spectral index used for scaling of extra-galactic component

A method of moments (MOM) code is used to simulate the radiation patterns and input impedance of each antenna under study. This code, called here the “patch code”, uses triangular patches to discretize a planar surface. Therefore it is able to calculate the current distribution on a planar antenna (such as the “blade”) more accurately and efficiently than a wire code such as NEC. This code allows an infinite ground to be included beneath the antenna, either perfectly conduction or lossy. The lossy ground is modeled using the reflection coefficient approximation. More information and a comparison of the results given by this code and other simulation codes are given in [7].

A C program was written to perform the calculations described above in order to generate expected drift scan curves. This program performs the following operations for each observation frequency:

- Load antenna radiation pattern data from file. Normalize as needed.
- Load sky map data from file.
- Scale sky map to observation frequency using specified scaling scheme.
- For each time step t
 - For each pixel in map (defined by indices i and j):
 - Convert pixel coordinates from galactic to azimuth and elevation relative to antenna given geographic coordinates of antenna, orientation of antenna, and time of day
 - If current pixel above local horizon, add power contributed by pixel (pixel temperature*normalized gain of antenna in same direction) to total received power for time t .
 - Scale power summed over whole map by mismatch loss and ground loss

Routines from the libnova C library [8] are used to perform the necessary coordinate conversions. Pattern data for the antenna is calculated in a relatively dense grid of 1° steps in both elevation and azimuth. In this way, the antenna gain in the direction of a given map pixel can be approximated by simply assuming the gain at the closest pattern grid point rather than needing to perform interpolation on the pattern data.

Drift Scan Measurement Approach

The setup shown in Figure 1 was used to perform drift scan measurements on each antenna under test. A dipole is connected to a Hicks active balun, and fed via 60 m of low-loss coaxial cable to a bias-T, which provides power to the balun. The output of the bias-T is connected to a bandpass filter with low and high cutoff frequencies of roughly 20 MHz and 80 MHz. This filter is used to reduce the received power due to out of band RFI in order to avoid generation of intermodulation products and/or saturation in downstream components. The output of the filter is fed to a gain stage and then to a spectrum analyzer. A laptop is used to capture data from the spectrum analyzer.

The spectrum analyzer is used to measure total power over the frequency range of 20 MHz to 80 MHz once every 5 minutes for a period of at least two consecutive days. The spectrum analyzer sweeps over the 20 MHz to 80 MHz band in a number of 6 MHz sub-sweeps, with 600 points per sub-sweep, and an RBW = 10 kHz. Within each sub-sweep, a 50 point video average is taken to reduce measurement noise. Data is recorded on the spectrum analyzer in linear format.

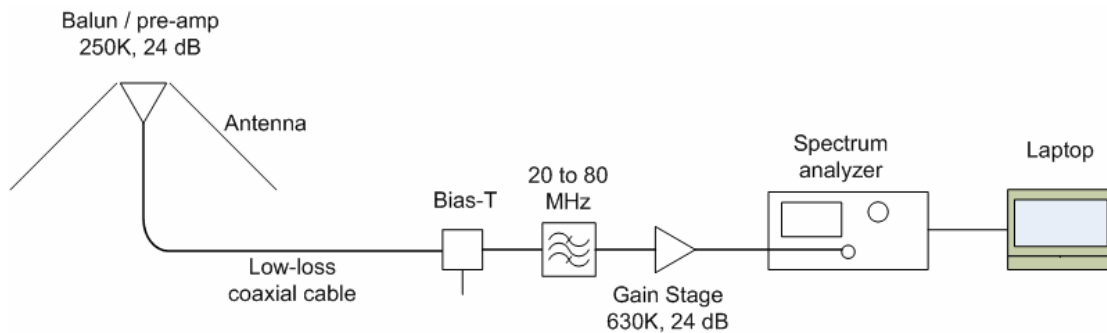


Figure 1. Test setup used for drift scan measurements.

A Y-factor measurement is performed in order to determine the gain and noise temperature of the test setup. It is important to perform this calibration so that an absolute comparison between simulated and measured drift scan data can be made. The calibration consists of connecting a noise diode with a known noise temperature at the balun input and taking total power measurements over the operating band. The noise diode is then turned off, and the measurements are repeated. These two sets of measurements are combined to determine a gain and noise calibration for the test setup. While these measurements were performed in-situ at least once during each drift scan measurement campaign, it was found necessary to perform extended Y-factor measurements of the test setup in the laboratory in order to reduce the uncertainty in the calibration to an acceptable level. This is due to the relative slow sample rate of the spectrum analyzer. The laboratory measurements, however, are believed to provide a representative calibration for drift-scan measurements since the Hicks balun has been shown previously to be relatively insensitive to changes in ambient temperature [9].

In this study, measurements were performed with the antenna operating directly over the ground without a ground screen. Without a ground screen, the conductivity and permittivity of

ground seen by the antenna may vary significantly depending upon the moisture of the soil (which varies with the amount of rainfall.) Therefore, measurements of ground parameters were made at least once during each drift scan measurement campaign using the ground probe method described in [10]. These measured ground parameter values are then used in the drift scan simulations so that a more representative comparison between measurement and simulation can be made. Between two different measurement campaigns roughly 4 weeks apart, the average conductivity and relative permittivity over 20 MHz to 80 MHz, varied between 0.007 S/m and 0.01 S/m and 5.3 and 6.9, respectively for the same site. This demonstrates that the ground parameters can vary significantly with time and that the values at a given site may be significantly different than the “average” values typically assumed in simulation.

A relatively simple procedure is used to process the raw drift scan measurement data. A raw data file, which corresponds to a single sweep over the 20 MHz to 80 MHz band, is read in and data editing and averaging is performed. This entails sub-dividing the data into a number of bins, each generally 50 points or 500 kHz in width, and performing iterative outlier removal in an attempt to remove RFI and calculating the mean for each bin. The noise / gain calibration determined previously for the test setup is then used to remove the effect of system noise from the measured noise temperature, which in principal leaves only the contribution due to sky noise, and references the measurement to the antenna terminals. This correction is accomplished using the following expression

$$T_{ANT} = \frac{T_{OUT} - G_{SYS}T_{SYS}}{G_{SYS}}$$

where T_{ANT} is the temperature due to the sky noise at the antenna terminals, T_{OUT} is the total temperature (due to sky and system noise) measured at the spectrum analyzer, G_{SYS} is the system gain, and T_{SYS} is the system temperature referenced to the input of the balun. This correction is applied individually for each bin.

Comparison of Simulated and Measured Drift Scan Results

Drift scan measurements were performed in the Spring of 2007 in order to validate the results of a study in which multi-objective genetic algorithm (GA) optimization was applied to the designs of antennas for LWA [11]; the two objectives considered in this study were sky noise frequency response and radiation pattern quality over the LWA frequency band. Measurements were performed on two different dipole antenna designs, the “big blade”, and one of the designs generated by the GA. The constructed versions of these two designs are shown in Figure 2. The GA-generated design shown was predicted to provide improved sky noise reception over the LWA band compared with the big blade at the expense of somewhat worse radiation patterns.

The measurements were performed in a rural area roughly 35 miles southwest of downtown Austin. The peak RFI levels measured at this site were generally at least 30 dB lower than in the city. The antennas were placed in a relatively open area at this site to provide good sky coverage. Measurements of the two antenna designs were performed over two separate weekends: big blade 4/20/07-4/22/07 and the GA design 5/04/07-5/06/07.

Simulated and measured drift scan data, presented in terms of the sky noise temperature component referenced to the antenna terminals, T_{ANT} , are compared as a function of frequency for the two antenna designs at two different points in time, 13:00 LST and 23:00 LST, in Figure 3. Simulated results in these plots were generated using the alternative map scaling scheme



Figure 2. Antennas designs used for drift scan study: big blade (above) and GA-generated design (below). The overall length and height of the big blade is 2.6 m and 1.5 m, respectively. The overall length and height of the GA design is 3.7 m and 1.2 m, respectively.

described above. No additional scaling has been applied to any of the data in these plots. Apart from the large spike due the TV channel 2 between 50 and 60 MHz, the measurement data for both antennas above 50 MHz is relatively RFI-clean. Below 50 MHz, however, RFI appears to be present at nearly every frequency, though in some cases it appears to cause the measured noise temperature to be only 1 dB or less higher than the expected sky noise temperature. There does appear to be a relatively clean bin near the low end of the measurement band for both antennas, however, around 22.5 MHz. Above 50 MHz, good agreement is seen between measurement and simulation for both designs and at both times. As expected, the GA design exhibits improved sky noise reception compared with the big blade at higher frequencies. At intermediate frequencies, a comparison between simulation and measurement cannot be made due to the RFI that is present in these bands nearly all of the time at the site. At 22.5 MHz, an offset between simulation and measurement is evident for both designs. This bias is believed to be due, at least in part, to error in the simulated ground loss calculation due to the approximate reflection coefficient-based ground model implemented in the patch code; the accuracy of this

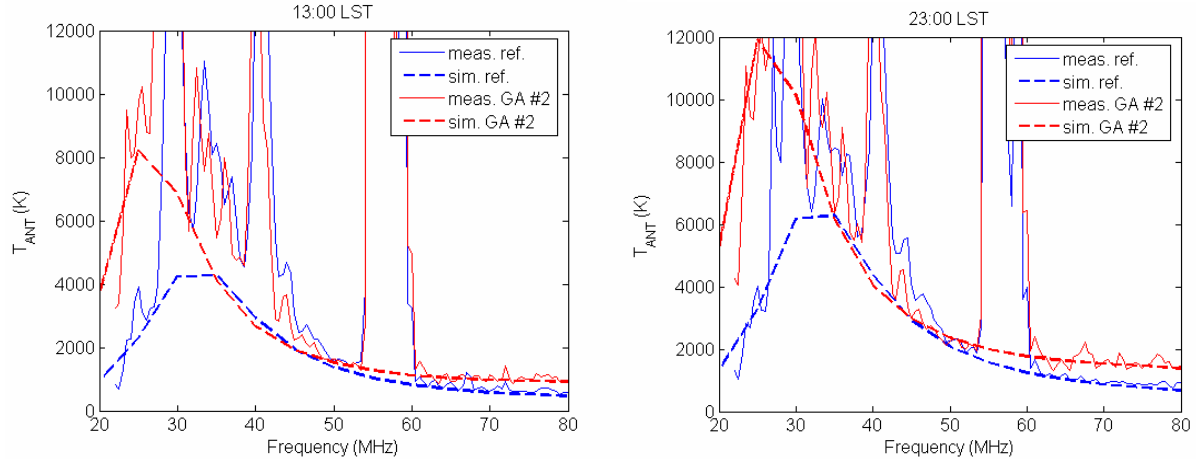


Figure 3. Comparison of simulated and measured drift-scan data for the big blade (denoted as “ref.” in the legends) and GA design as a function of frequency at 13:00 LST and 23:00 LST.

ground model will tend to be worse at lower frequencies than at higher frequencies. Despite this limitation, the offset appears to be roughly consistent between the two antenna designs. Therefore as predicted by simulation, the measured sky noise for the GA design at lower frequencies is significantly higher than the big blade.

The simulated and measured drift scan data as a function of time are compared in Figures 4 and 5 for the big blade and GA design at the four cleanest frequency bands, 22.5 MHz, 50 MHz, 65.5 or 70 MHz, and 79 MHz. Simulated results in these figures were generated using both the original (“orig. scale” in the plot legends) and the alternative (“new scale” in the plot legends) map scaling schemes described above. At each frequency, an additional scaling factor has been applied to each of simulated results in order to achieve the best possible fit with the measured data. This scaling was performed manually, trying to take into account what features of the measurements appear to be due to sky noise and what appear to be due to RFI. This approach is clearly somewhat subjective, but provides a preliminary means of assessing the level of absolute agreement between simulation and measurement. The additional scaling factors applied to simulation results are noted in the legends of each plot in Figures 4 and 5.

Despite haven chosen the cleanest measurement bands available, it can be seen in Figures 4 and 5 that significant RFI remains, particularly at the lowest band 22.5 MHz. While some of this is likely due to intermittent terrestrial RFI, the appearance of interference across the entire 20 to 80 MHz band (for instance, note the sustained increased noise levels between 25:00 and 35:00 LST that are apparent in all big blade measurements) suggests that lightning was nearby. It is known that thunderstorms were in the vicinity of the test site during both measurement campaigns. Despite these limitations, there appears to be an extended period of relatively clean data in both data sets: 37:00 to 51:00 for the big blade and 37:00 to 55:00 for the GA design for most frequencies. In these clean periods, it is apparent that the shapes of the simulated drift curves agree relatively well with those of the measured drift curve over all frequencies and for both designs. The curves generated using the alternative map scaling scheme, however, appear to provide better agreement in shape than the original map scaling scheme. A good example of this is exhibited at 49.5 MHz and 65.6 MHz for the GA design where the original scaling predicts more flattened peaks near 43:00 LST compared with the more rounded peaks predicted

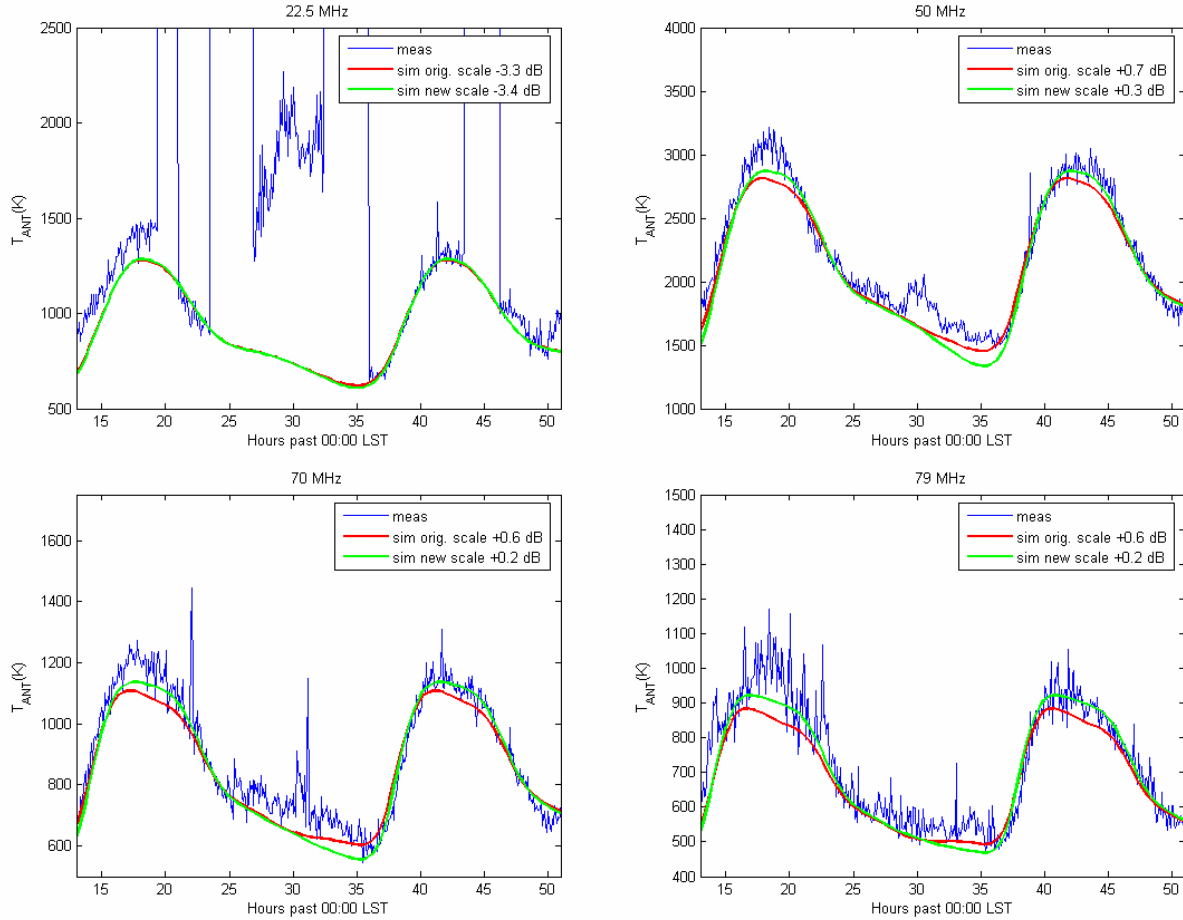


Figure 4. Comparison of simulated and measured drift scan data as a function of time for big blade at 22.5 MHz, 50 MHz, 70 MHz, and 79 MHz.

by the alternative scaling, which appears to agree better with the measured curves. Note that this difference in simulated curve shapes is indeed due to the difference in map scaling since identical radiation patterns were used in both simulations. The level of agreement between measured and simulated curve shapes suggest that the simulated radiation patterns are relatively accurate.

As expected after consideration of Figure 3, relatively large additional scaling factors, roughly -3.5 dB for both designs and map scalings, were applied to simulations to achieve good agreement with measurement at 22.5 MHz. Over all other frequencies, and between the two designs and both map scalings, however, a good fit was achieved by applying a scale factor of 0.7 dB or less in amplitude. This suggests that, particularly at higher frequencies, simulation provides a good estimate of both mismatch loss and ground loss. It also suggests that both map scaling schemes provide a reasonable estimate of the absolute received sky noise power level. For the big blade design, the best fit scale factors for the alternative scaling were smaller in amplitude at all frequencies above 22.5 MHz than those for the original scaling. On the other hand with the GA design, the best fit scale factors were slightly smaller in amplitude for the original map scaling than the alternative scaling. This variation in results can be explained in part by the subjectivity inherent in the manual method to determine best fit offsets. For example,

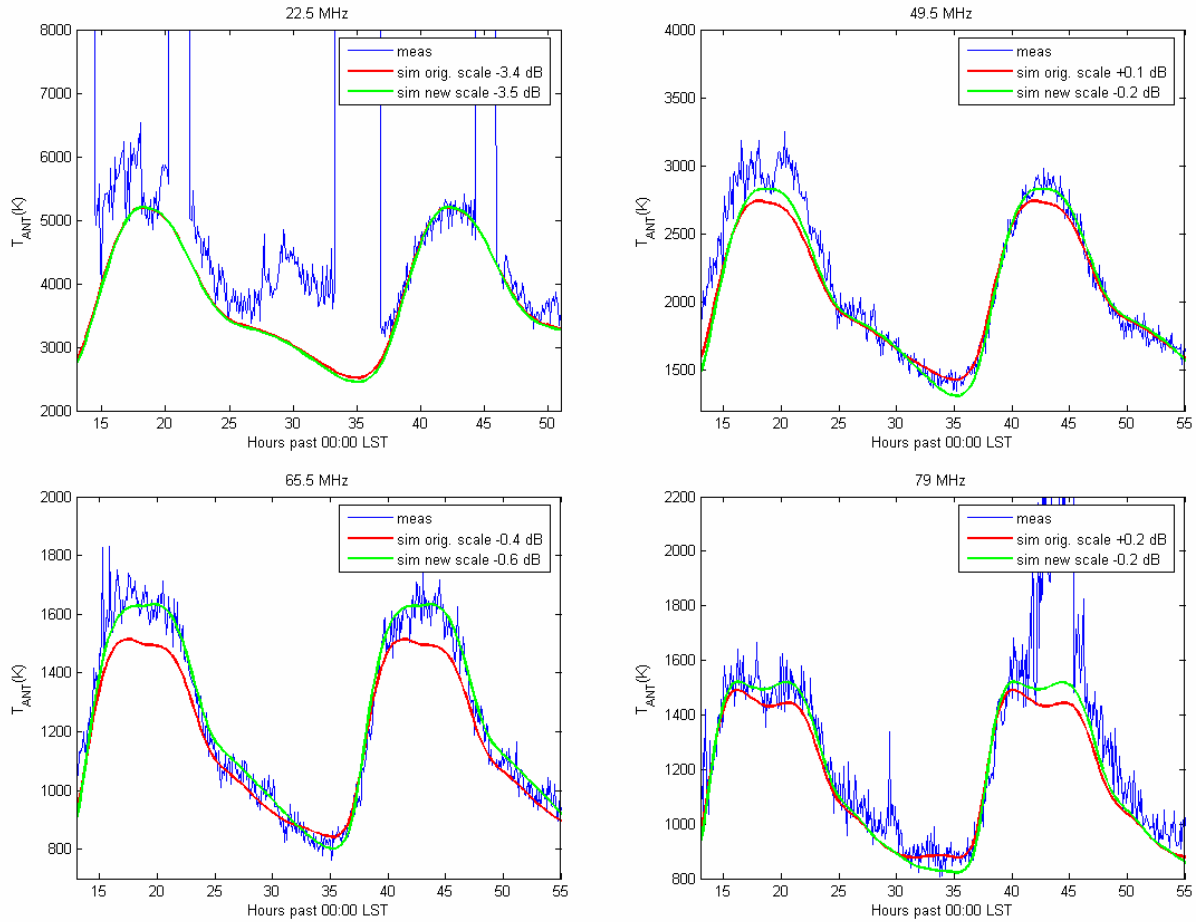


Figure 5. Comparison of simulated and measured drift scan data as a function of time for big blade at 22.5 MHz, 49.5 MHz, 65.5 MHz, and 79 MHz.

since the shape of the curves generated using the original map scaling deviated noticeably from the measured curves, significantly different offsets result by trying to fit the simulated and measured curves near the null of the curves (as was done in Figures 4 and 5) compared with near the peak of the curves.

Comparison of simulated and measured results is complicated by a number of other issues as well. There are some effects present in measurement, which have not been accounted for in simulation in the results presented above. For instance, it is known that the antenna mounting structure has some effect on the antenna performance. Through measurement, it was found that the mismatch loss of the big blade pictured in Figure 2 above could be changed by up to 0.3 dB within the LWA band by removing the mast and mounting plate; the proper shape of the antenna was held by the lower arm supports shown in the figure and rope. In the results presented above, the mean conductivity and permittivity measured over 20 to 80 MHz for each drift scan measurement campaign was used in performing simulations at all frequencies in the band. It is expected that the ground loss calculation at the high and low frequencies in the band could be affected at the 0.2 dB level by using the actual measured ground parameters rather than the mean values at each frequency; additionally there could be some error in the ground parameter measurements themselves. Although it seems like the effects of HII absorption, as

discussed in [12], should be included in the alternative map scaling approach presented in this paper, it is not readily apparent to the author that this is really the case.

There are a number of potential sources of bias in the sky noise measurements. Fortunately, most of these are accounted for by performing the Y-factor calibration for system noise and gain. However, this calibration is completely dependent upon the assumed noise temperature of the noise diode used in measurement. Independent measurements of the noise diode used in this study suggest that the noise temperature it outputs is within ± 0.2 dB of the vendor supplied calibration of the device over 20 to 80 MHz. However, the methods used to make this determination were not extremely rigorous. Finally, measurement uncertainty is a problem. Due to the relatively slow sample rate of the spectrum analyzer used in this study, significant measurement noise remains in the final results. This and the relatively short data collection period used (2 days) make it more difficult to discern sky noise from low-level RFI.

Conclusions

The results of a comparison of measured and simulated drift scans using wideband dipole antennas over the LWA band have been presented. Calibrated total power measurements were taken with two different antenna designs, each over a period of two days. Simulated drift scans were generated for each antenna design by convolving simulated radiation patterns with a frequency scaled all-sky map of the radio continuum; ground parameters measured at the drift scan measurement site were used in simulation to calculate ground loss. Simulation results were presented for two different sky map frequency scaling approaches: 1) the typical scheme in which the sky map is scaled by a single factor between the map and observation frequency, and 2) an alternative scheme in which the original map is decomposed into galactic, extra-galactic, and cosmic microwave background components, which are individually scaled as needed, to the observation frequency using scaling parameters given in [6]. There was found to be an offset between simulated and measured drift scans near the low end of the LWA band (22.5 MHz) of roughly 3.5 dB, which is presumed to be due at least in part to error in the simulated ground loss calculation. However, at higher frequencies (50 MHz and above), agreement of better than 0.7 dB was achieved between measurement and simulations using both map scaling approaches. The alternative scaling scheme presented, however, appears to provide better agreement with measurement in terms of the shape of the drift scan curves.

While the results presented here are promising in terms of the level of agreement apparently achieved between simulated and measured drift scans, a number of improvements could be made to the procedures used in order to better characterize the absolute accuracy of simulation. The single biggest improvement in the measurement procedure would be to perform measurements in a more RFI-quiet environment such as the LWDA site. It would also be useful to collect high sample rate (MSPS-level) total power data if a receiver that operated over the full 20 to 80 MHz band were available. It is particularly important to cover the band below 50 MHz in these measurements since RFI was nearly always present at most of these frequencies at the central Texas measurement site, which prevented a comparison of simulation and measurement results. Use of a high sampling rate receiver rather than a traditional spectrum analyzer would significantly reduce measurement noise so that low-level RFI could be more easily discerned from sky noise. It would be useful to perform measurements over a much longer period, on the order of weeks, so that periods of high interference could be easily filtered from the data set. This would make it easier to apply formal data fitting techniques in order to assess the accuracy

of simulations. If the focus of study is the absolute accuracy of a particular sky map scaling scheme, it would be better to remove the uncertainty associated with a lossy ground by installing a large ground screen beneath the antenna. A very large ground screen (much larger than that needed to stabilize input impedance), however, would be required in order to recover all of the ground loss (to less than 0.1 dB). Finally, in the assessment of absolute accuracy of simulation results, it is critical that a Y-factor calibration of system gain and noise be performed using a well characterized noise source at least once during each drift scan measurement campaign.

Improvements could certainly be made to the simulation approach as well. It would be desirable to achieve better accuracy in the simulated ground loss calculation at low frequency, which in the case of the patch code would require adding a Sommerfeld-type ground model (a significant effort); if non-planar, wire-based antennas are being considered, then NEC should provide reasonable accuracy in this regard. If large ground screens are used in measurement, however, then this is not an issue. Including the effects of antenna mounting hardware will improve the accuracy of antenna simulations. There are perhaps more appropriate sky map scaling parameter values than those given in Table 1; a thorough literature search has not been performed in this regard. Better yet, if sky maps of spectral index, such as those described in [6] are available, perhaps it would be possible to scale each pixel of the sky map of brightness temperature individually to attain the highest possible accuracy; it is not clear how practical this would be, however. Finally, if they are not already properly included in simulation, the effects HII absorption should be considered.

References

- [1] A.E.E Rogers, P. Pratap, E. Kratzenberg, "Calibration of active antenna arrays using a sky brightness model", *Radio Sci.*, vol. 39, RS2023, 2004.
- [2] C.G.T Haslam *et al.*, "A 408 MHz all-sky continuum survey. II. The atlas of contour maps," *Astron. Astrophys. Suppl. Ser.*, vol. 47, pp. 1-143, Jan. 1982.
- [3] Haslam 408 MHz all-sky map downloaded from: <http://adil.ncsa.uiuc.edu/document/95.CH.01.01>
- [4] fv FITS viewer available at: <http://heasarc.gsfc.nasa.gov/ftools/fv/>
- [5] S. Ellingson, H. Simonetti, C. Patterson, "Design and evaluation of an active antenna for a 29-47 MHz radio telescope array", *IEEE Trans. Antennas Propag.*, vol. 55, pp. 826-831, Mar. 2007.
- [6] K. Lawson, C. Mayer, J. Osborne, M. Parkinson, "Variations in the spectral index of the galactic radio continuum emission in the northern hemisphere", *Mon. Not. R. astr. Soc.*, vol. 225, pp. 307-327, 1987.
- [7] A. Kerkhoff, "Multi-objective genetic algorithm optimization of antennas for use in LWA", *LWA memo 64*, Nov. 2006.
- [8] libnova library available at <http://libnova.sourceforge.net/>
- [9] R. Bradley, C. Parashare, "Evaluation of the NRL LWA Active Balun Prototype", *Report 01, Rev A*, originally dated Feb. 2005.
- [10] G. Smith, J. Nordgard, "Measurement of the electrical constitutive parameters of materials using antennas", *IEEE Trans. Antennas Propag.*, vol. 33, July 1985, pp. 783-792.
- [11] A. Kerkhoff, H. Ling, "Application of pareto genetic algorithm optimization to the design of broadband dipole elements for use in the Long Wavelength Array (LWA)", *2007 IEEE AP-S Int'l Symp.*, Honolulu, HI, June 2007.
- [12] B. Erickson, "HII absorption", *LWA memo 77*, Nov. 2006.